# *Impact of the North Atlantic Oscillation on transatlantic flight routes and clear-air turbulence*

Article

Accepted Version

## www.reading.ac.uk/centaur

## CentAUR

Central Archive at the University of Reading

Reading's research outputs online

1 **Impact of the North Atlantic Oscillation on Transatlantic**

2 **Flight Routes and Clear-Air Turbulence**

3

4

5 Jung-Hoon Kim[1], William N. Chan[2], Banavar Sridhar[2], Robert D. Sharman[3],

6 Paul D. Williams[4], and Matt Strahan[5]

7

8

9 *Cooperative Institute for Research in the Atmosphere, Colorado State University, in*

10 *affiliation with NOAA/NWS Aviation Weather Center, Kansas City, Missouri, USA[1]*

11 *NASA Ames Research Center, Moffett Field, California, USA[2]*

12 *National Center for Atmospheric Research/Research Application Laboratory, Boulder,*

13 *Colorado, USA[3]*

14 *Department of Meteorology, University of Reading, Reading, United Kingdom[4]*

15 *NOAA/NWS Aviation Weather Center, Kansas City, Missouri, USA[5]*

16

17

20

21

22 *Corresponding Author*: Dr. Jung-Hoon Kim, 7220 NW 101st Terrace, Kansas City,

23 Missouri, 64153-2317, E-mail: jung-hoon.kim@noaa.gov; jhkim99@me.com

**1  Abstract**

2     The variation of wind-optimal transatlantic flight routes and their turbulence

3  potentials is investigated to understand how upper-level winds and large-scale flow

4  patterns can affect the efficiency and safety of long-haul flights. In this study, the Wind-

5  Optimal Routes (WOR) that minimize the total flight time by considering wind

6  variations are modeled for flights between John F. Kennedy international airport (JFK)

7  in New York and Heathrow airport (LHR) in London during two distinct winter periods

8  of abnormally high and low phases of North Atlantic Oscillation (NAO) teleconnection

9  patterns. Eastbound WORs approximate the JFK-LHR Great Circle (GC) route

10  following northerly shifted jets in the +NAO period. Those WORs deviate southward

11  following southerly shifted jets in the –NAO period, because eastbound WORs fly

12  closely to the prevailing westerly jets to maximize tail winds. Westbound WORs,

13  however, spread meridionally to avoid the jets near the GC in the +NAO period to

14  minimize head winds. In the –NAO period, westbound WORs are north of the GC

15  because of the southerly shifted jets. Consequently, eastbound WORs are faster but

16  have higher probabilities of encountering Clear-Air Turbulence (CAT) than westbound

17  ones, because eastbound WORs are close to the jet streams, especially near the cyclonic

18  shear side of the jets in the northern (southern) part of the GC in the +NAO (-NAO)

19  period. This study suggests how predicted teleconnection weather patterns can be used

20  for long-haul strategic flight planning, ultimately contributing to minimizing aviation's

21  impact on the environment.

**1. Introduction**

Emissions from en-route commercial aircraft are a significant anthropogenic contribution to global warming as air transportation over the globe grows rapidly (e.g., Lee et al. 2009; 2010). From an operational perspective, a method to reduce these emissions is to optimize flight routes in the presence of wind variations, which minimizes the total travel time and fuel consumption (e.g., Sridhar et al. 2011; Kim et al. 2015). This Wind-Optimal Route (WOR) is regarded as an efficient and environmentally friendly flight route because the amount of airborne emissions is simply a function of fuel usage, which is approximately proportional to travel time, although other factors like $NO_x$, $O_3$, water vapor, and contrail formation need to be considered for the total climate impact (e.g., Grewe et al. 2014). These efficient WORs may not be viable if Clear-Air Turbulence (CAT) is embedded near upper-level jets, because CAT causes safety issues and must be avoided. For commercial aircraft, CAT encounters are the leading cause of in-flight injuries among all weather-related incidents (e.g., Sharman et al. 2006). As international air traffic density increases dramatically, problems like economical costs for injuries, cabin and structural damage, and flight delays become significant. Therefore, it becomes necessary to develop routes that minimize both fuel use and the potential for CAT encounters.

Several strategies have been developed to determine WORs for air traffic management (ATM) but they do not take into account turbulence. For example, Ng et al. (2012) developed and computed WORs at multiple flight levels, which minimized total flight times by taking into account the variations of upper-level winds. Pilot behaviors during turbulence encounters and their impact on ATM has been well documented by Krozel et al. (2011), showing that CAT avoidance maneuvers are depend on aircraft

3

type and company policies. Since most of the moderate-or-greater (MOG)-level CAT

encounters occur near the upper-level jet and frontal systems (e.g., Lester 1994; Wolff

and Sharman 2008; Kim and Chun 2011), flight routes that approach a jet to benefit

from tail winds may incur extra fuel uses to avoid adverse turbulence encounters (e.g.,

Williams and Joshi 2013; Kim et al. 2015).

For long-haul transatlantic flights, WOR trajectories depend on the prevailing jet

stream position and strength. Transatlantic WORs are known to be changing as the jet

stream responds to climate change (Williams 2016). The CAT potential along these

trajectories also depends upon weather conditions because local gradients of horizontal

and vertical wind and temperature are generally large near the jet stream (e.g., Jaeger

and Sprenger 2007; Williams and Joshi 2013; Karnauskas et al. 2015). The North

Atlantic Oscillation (NAO) is one of the most prominent teleconnection patterns, which

is composed of a north-south dipole pattern of height or pressure anomalies over the

North Atlantic, especially in winter time (e.g., Wallace and Gutzler 1981; Barnston and

Livezey 1987). In the positive phase of the NAO (hereafter referred to as +NAO),

stronger pressure gradients between the persistent subtropical high and Icelandic low

lead to a higher-latitude position of the jet stream. Weaker gradients in the negative

phase of the NAO (hereafter -NAO) shift the jet stream further south, which can create

different flight trajectories and environmental impacts (Irvine et al. 2012) as well as

different CAT probabilities (Jaeger and Sprenger 2007). Therefore, this study aims to

investigate how upper-level jet stream characteristics associated with the NAO can lead

to variations in long-haul transatlantic flight routes and their CAT potentials. This

information can be used for efficient and safe decision making, while also minimizing

aviation's impact on the environment.

1    Section 2 describes the modeling of WOR trajectories, and section 3 examines

2    deviations of the transatlantic WORs and their CAT potentials during two winter

3    seasons with distinct NAO patterns. The summary and conclusions are discussed in

4    Section 4.

5

6    **2. Modeling of Wind-Optimal Route (WOR) aircraft trajectories**

7        When an aircraft is flying horizontally above the Earth's surface with a true

8    airspeed $V_t$ and heading angle $\alpha$ during a certain period of time $\Delta t$, as shown in Fig. 1,

9    the longitudinal $\lambda$ and latitudinal $\phi$ position changes of the aircraft with time in the

10   presence of horizontal winds are governed by the following aircraft-motion equations

11   (e.g., Sridhar et al. 2011; Ng et al. 2012; Kim et al. 2015):

$$\frac{d\lambda(t)}{dt} = \frac{V_t \cos\alpha(t) + u(\lambda, \phi, z)}{R \cos\phi(t)}, \qquad (1)$$

$$\frac{d\phi(t)}{dt} = \frac{V_t \sin\alpha(t) + v(\lambda, \phi, z)}{R}. \qquad (2)$$

12       Here, $R$ is the Earth's radius (the Earth is assumed to be a sphere), $z << R$ is the

13   height above the surface, and $u$ and $v$ are the zonal and meridional wind components,

14   respectively. $V_t$ is a constant of 250 m s$^{-1}$ (which is representative of the general

15   airspeed of commercial flight).

16       To maximize the advantage of a tail wind and/or minimize the disadvantage of a

17   head wind in the modeling of an aircraft trajectory, we need to take into account wind

18   variations in the calculation of the heading angle ($\alpha$) at each time step to minimize the

19   total travel time from departure to destination. To compute the WOR, the aircraft

20   heading angle ($\alpha$) is regarded as a control parameter. Then, the analytic solution of $\alpha$

21   that minimizes the total cost function in Eq. (3) (i.e., total travel time) is derived by

1    Pontryagin's Minimum Principle (Bryson and Ho 1975).

$$J = \int_{t_0}^{t_f} C_t \, dt. \qquad (3)$$

2        Here, $C_t$ is the cost coefficient of travel time ($C_t = 1$ in this study), and $t_0$ and $t_f$ are

3    the times at the departure and arrival airports, respectively. The analytic solution for the

4    control parameter of heading angle ($\alpha$) that takes into account the variations of the

5    winds in Eqs. (1, 2) and minimizes the total cost function in Eq. (3) is:

$$\frac{d\alpha(t)}{dt} = -\frac{F_{wind}(t)}{C_t \, R \, cos\phi(t)}, \qquad where$$

$$F_{wind}(t) = -sin\,\alpha(t)\,cos\,\alpha(t)\frac{\partial u(\lambda, \phi, z)}{\partial\lambda} + cos^2\alpha(t)\,sin\,\phi(t)\,u(\lambda, \phi, z)$$

$$+ cos^2\alpha(t)\,cos\,\phi(t)\frac{\partial u(\lambda, \phi, z)}{\partial\phi} - \frac{\partial v(\lambda, \phi, z)}{\partial\lambda}$$

$$+ sin\,\alpha(t)\,cos\,\alpha(t)\,sin\,\phi(t)\,v(\lambda, \phi, z)$$

$$+ cos\,\alpha(t)\,sin\,\alpha(t)\,cos\,\phi(t)\frac{\partial v(\lambda, \phi, z)}{\partial\phi} + V_t\,cos\,\alpha(t)\,sin\,\phi(t)$$

$$+ cos^2\alpha(t)\,\frac{\partial v(\lambda, \phi, z)}{\partial\lambda}. \qquad (4)$$

6        A full derivation of the analytic solution in Eq. (4) can be found in previous studies

7    (e.g., Sridhar et al. 2011; Ng et al. 2012; Kim et al. 2015). In the next stage, the optimal

8    initial heading angle [$\alpha(t_0)$] at the departure airport is determined as follows. First, the

9    Great-Circle heading angle ($\alpha_{GC}$) between the departure and arrival airports is selected

10   as a first guess for the optimal heading angle (Kim et al. 2015). Then, Eqs. (1), (2), and

11   (4) are solved using the explicit Euler forward integration scheme, [$y(t + 1) = y(t) +$

12   $\Delta t \frac{dy(t)}{dt}, where \; y = \lambda, \phi, and \; \alpha.$] from the departure to the destination. This process is

13   iterated with different initial heading angles [$\alpha(t_0)$] ranging between $\alpha_{GC} - 45°$ and $\alpha_{GC}$

6

1   + 45° with an increment of 2.5° until each trajectory meets the termination condition of

2   either: 1) The minimum distance between the trajectory and final destination is smaller

3   than 100 km, or 2) The distance between each trajectory and the initial departure airport

4   is greater than 1.2 × total Great Circle distance between the departure and arrival

5   destination. Finally, amongst these, the trajectory that arrives at the destination faster

6   than any of the others is chosen as the WOR. As the true air speed ($V_t$) is fixed in Eqs.

7   (1) and (2) in this study, the calculated WOR is time optimal at a given flight level.

8      Figure 2 shows an example of the WOR calculations for eastbound (EB) and

9   westbound (WB) routes at 250 hPa (about $z = 11$ km) between the John F. Kennedy

10   international airport (JFK) in New York and Heathrow airport (LHR) in London for 00

11   (left) and 12 (right) UTC on 3 January 2005. In this example, wind data are from the 6-

12   hourly Modern Era Retrospective-analysis for Research and Application (MERRA)

13   reanalysis data with 2/3° (longitude) × 1/2° (latitude) horizontal grid spacing. The time

14   step ($\Delta t$) = 180 seconds (3 minutes) for the trajectory modeling by Eqs. (1), (2), and (4)

15   with $V_t$ of 250 m s$^{-1}$, which roughly corresponds to the resolution of MERRA wind data.

16   EB (gray lines in Fig. 2 upper left) and WB (gray lines in Fig. 2 upper right) trajectories

17   reach different regions according to the initial heading angles selected [$\alpha(t_0)$] in a given

18   wind situation, which corresponds to the minimum distance between each trajectory and

19   the destination in Fig. 2 (lower). The fastest one to the destination has been picked up as

20   the EB WOR (blue-bold line in Fig. 2 upper left) and WB WOR (red-bold line in Fig. 2

21   upper right) in this wind condition. For a reference, the Great Circle (GC) route between

22   JFK and LHR is depicted as black bold line.

23      The total flight time along this GC with still air (no wind) would be 368 min with $V_t$

24   of 250 m s$^{-1}$. In this case, the EB WOR (blue line) follows the strong westerly and

7

1    southwesterly jet over the North Atlantic to maximize its tail wind (Fig. 2 upper left;

2    321 min of total flight time). The WB WOR (red line) detours northward near the

3    southern tip of Greenland to avoid the prevailing westerly jet flow, thereby minimizing

4    its head wind (Fig. 2 upper right; 417 min of total flight time). It is noted that in Fig. 2

5    (right) the WB trajectory with the initial heading angle of the GC routes (162º) doesn't

6    go directly to JFK and has a longer flight time than two other WB trajectories as it

7    avoids the jet stream. In this case, the northerly route with $\alpha(t_0) = 154.5º$ (red line) is

8    selected as the WB WOR because this is 1 min faster than the southerly detouring one

9    with $\alpha(t_0) = 172º$ to the JFK in a given wind condition.

10

11   **3. Results**

12      Variations of the WORs and their CAT potentials between the JFK and LHR are

13   investigated during two distinct winter seasons [December 2004 – February 2005

14   (DJF04-05) and December 2009 – February 2010 (DJF09-10)]. The two seasons are

15   selected because monthly averaged values of the NAO index in DJF04-05 are highly

16   positive (+1.21 in December and +1.52 in January), while they are extremely negative

17   in DJF09-10 (-1.92 in December and -1.11 in January) according to the Climate

18   Prediction Center (CPC). These periods were already selected for the study of aviation's

19   impact on the environment based on weather patterns in Irvine et al. (2012).

20      Figure 3 shows the averaged horizontal wind speed (upper), variability of the EB

21   (blue lines; middle) and WB (red lines; lower) WORs at 250 hPa during DJF 04-05 (left)

22   and DJF 09-10 (right). In this study, the EB (WB) WORs are launched at 00 (12) UTC

23   each day during the study periods, which corresponds to a maximum of actual air traffic

24   in the North Atlantic corridor (Schumann and Graf 2013), and the route between JFK

1 and LHR is selected as a representative transatlantic flight route (Irvine et al. 2012).

2 Figures 3a and b show distinct jet streams in two different NAO phases. Due to the

3 interannual variability of persistent high and low pressure systems in the North Atlantic,

4 the dominant jet stream shifts northward direct to northwestern Europe in +NAO (Fig.

5 3a), and moves southward closer to southern Europe in -NAO, which is consistent with

6 previous studies (e.g., Barnston and Livezey 1987; Jaeger and Sprenger 2007; Irvine et

7 al. 2012).

8    In Figs. 3c-f, the overall features of the EB (blue lines in c and d) and WB (red lines

9 in e and f) WORs are different between the two designated winter seasons. The EB

10 WORs from JFK to LHR usually follow the prevailing westerly jet stream to maximize

11 tail winds, thereby reducing total travel time and fuel consumption. In particular, the EB

12 WORs are close to the GC between JFK and LHR (a reference black line) and

13 distributed both north and south directly to Northern Europe following northerly shifted

14 jets in the +NAO phase during DJF04-05 (Fig. 3c). EB WORs are more southerly

15 toward Southern Europe and the Mediterranean Sea (Fig. 3d), following the southerly

16 shifted jet streams in the –NAO phase during DJF09-10 (Fig. 3b). These results are

17 consistent with the flight trajectories in weather pattern 2 in Irvine et al. (2012; Fig 7 in

18 their study). The WB WORs from LHR to JFK, however, avoid the prevailing westerly

19 jet stream to minimize their head winds. In the +NAO phase during DJF04-05 (Fig. 3e),

20 the WB WORs deviate southward or northward to avoid the strong jet stream

21 dominating along the GC, so that the envelope of the WB WORs becomes meridionally

22 spread. However, in the –NAO phase during DJF09-10 (Fig. 3f), due to the southerly

23 shifted westerly jet stream, the WB WORs are mostly around the northern part of the

1    GC (Fig. 3f). This is similar to the trajectories of weather pattern 4 in Irvine et al. (2012;

2    Fig 7 in their study).

3        Figure 4 shows bar charts of the mean, ± 2 standard deviations, and maximum and

4    minimum values of the flight times for the EB and WB WORs during the +NAO

5    (DJF04-05; leftmost two) and –NAO (DJF09-10; rightmost two). First, EB WORs are

6    faster than WB WORs, as expected from Fig. 3. Second, the difference of total travel

7    time between EB and WB WORs is greater in the +NAO phase during DJF04-05 than

8    in the –NAO phase during DJF09-10, because the prevailing westerly jet along the GC

9    is stronger in +NAO than –NAO phases as shown in Figs. 3a and b. Third, EB WORs

10   (WB WORs) in +NAO (–NAO) phase are faster than those in –NAO (+NAO), because

11   distances of the EB WORs (WB WORs) are smaller in +NAO (–NAO) phase as well as

12   tailwinds (headwinds) are stronger in +NAO (–NAO) phase (Figs. 3c-f).

13       Based on the aforementioned variability of the WORs in each period, the difference

14   of CAT potentials along these WORs can be investigated using the MERRA data with

15   50 hPa vertical grid spacing between the 400 and 100 hPa levels, because grid-

16   resolvable strong vertical wind shears and temperature gradients can be a good indicator

17   for aircraft-scale turbulence (e.g., Sharman et al. 2006; Jaeger and Sprenger 2007; Kim

18   et al. 2011; Williams and Joshi 2013). Figure 5a and b show the averaged values of the

19   Turbulence Index 1 (TI1) for two winter times. The TI1 diagnostic is a combination of

20   vertical shear and total deformation, which is a simplified version of upper-level

21   frontogenesis that is a typical CAT generation mechanism, especially above and below

22   the jet core in the cyclonic shear-side of the jet streak (Ellrod and Knapp 1992). Thus, it

23   is most skillful and is the most widely used CAT indicator in operational forecasts (e.g.,

24   Sharman et al. 2006; Kim et al. 2011; Gill 2014).

$$TI1(x, y, z) = VWS(x, y, z) \times DEF(x, y, z), \qquad where$$

$$VWS(x, y, z) = \left\{ \left( \frac{\partial u(x, y, z)}{\partial z} \right)^2 + \left( \frac{\partial v(x, y, z)}{\partial z} \right)^2 \right\}^{1/2}, and$$

$$DEF(x, y, z) = \left\{ \frac{\partial v(x, y, z)}{\partial x} + \frac{\partial u(x, y, z)}{\partial y} \right\}^2 + \left\{ \frac{\partial u(x, y, z)}{\partial x} - \frac{\partial v(x, y, z)}{\partial y} \right\}^{1/2}.$$

1    In Figs. 5a and b, higher values of averaged TI1 index in northern parts of JFK-

2    LHR GC in +NAO and southern parts in –NAO correspond to the cyclonic shear-side of

3    the jets shown in Figs. 3a and b, which is more obvious in Fig. 5c for the difference of

4    the averaged TI1 between two periods. Considering the variations of EB and WB

5    WORs shown in Figs. 3c-f, the EB WORs would pass more frequently through higher

6    TI1 areas in both winter periods. As an example, Figure 5d shows a snapshot for the TI1

7    with horizontal wind vectors at 250 hPa during 3 January 2005. During this time, the

8    WB WOR (red line) passed through less area with higher CAT potentials, because it

9    deviates northward to avoid the prevailing westerly and southwesterly flows (it might

10   be also small when it would detour southward), while EB WOR (blue line) encountered

11   higher CAT potential areas for a longer period of time.

12   The Probability Density Functions (PDFs) for TI1 along the EB and WB WORs

13   during two winter times are investigated. Figure 6 shows PDFs for TI1 along the EB

14   (blue) and WB (red) WORs in +NAO (DJF04-05). Overlaps between EB and WB

15   WORs are depicted as orange-color bars. The median of EB WORs (blue; $23.4 \times 10^{-9}$ s$^{-2}$)

16   is higher than that of WB WORs (red; $21.5 \times 10^{-9}$ s$^{-2}$). Median values of the PDFs for EB

17   and WB WORs in two winter periods are summarized in Table 1. The probability of the

18   99th percentile value ($13.4 \times 10^{-8}$ s$^{-2}$) of TI1 – approximately representing moderate-or-

19   greater (MOG)-level CAT – has also been calculated and tabulated in Table 1. As

11

expected, the medians of CAT for EB WORs are higher than those of WB WORs in

both winter periods. The chances of encountering MOG-level CAT are also higher

along the EB WORs than WB WORs because they are following the jet stream where

CAT potentials are higher. Especially, EB WORs in –NAO have the highest chance

because most trajectories tend to pass directly to the cyclonic shear side of the southerly

shifted jet stream (e.g., Figs. 3d and 5b). For the WB WORs, the +NAO phase has a

higher median value and higher chances for MOG-level CAT because some of the WB

WORs detouring northward would encounter high CAT potential areas in the cyclonic

shear side of the northerly shifted jet stream in +NAO (e.g., Figs. 3e and 5a). For the

confidence test, 200 half-portions of the total TI1 data sample along the WORs have

been randomly selected to make the same PDFs, medians, and the MOG-level CAT

probabilities in Table 1. Among the 200, the maximum and minimum values of medians

and MOG-level CAT probabilities are within ±10% of the values in Table 1, which

shows that the results in Table 1 are statistically significant (e.g., Sharman et al. 2006;

Kim et al. 2011).


## 4. Summary and conclusions

   In this study, the variations of transatlantic WORs between JFK and LHR, and their

CAT potentials in two different winter seasons were investigated. Simplified aircraft

trajectory models were derived by applying the minimal principal theory to the control

parameter of aircraft heading angle in the presence of winds. Results show the

variability of WORs and their CAT potentials during two distinct upper-level flow

patterns. Depending on the upper-level winds, the modeled WORs had different flight

trajectories and flight times (and consequently fuel burned). EB WORs are close to the

GC between JFK and LHR by following northerly shifted jet streams in +NAO, while EB WORs deviate southward by taking advantage of the southerly shifted jets in –NAO. WB WORs, however, detoured northward or southward of the prevailing jets along the GC, which spreads out the trajectories meriodionally in +NAO, but those are along the GC in –NAO due to the southerly shifted jets. Eventually, EB WORs were faster than WB WORs. EB WORs in +NAO are faster than those in –NAO, because the jet stream along the GC is stronger in +NAO. EB WORs had a higher probability of encountering MOG-level CAT than WB WORs, as they pass through the higher regions of vertical and horizontal wind shears near the jet stream in both winter times. In particular, the EB WOR trajectories in the –NAO period are in phase with high CAT potentials in the cyclonic-shear side of the southerly shifted jets.

   This information can be used in the aviation sector to understand how the predicted upper-level teleconnection weather patterns can be translated to make a decision for safe and efficient long-haul transatlantic flight routes. For example, the predicted jet stream would be shifted northward in a +NAO pattern, so a pilot from JFK to LHR (i.e., EB) could fly in the anticyclonic shear side of the jet streak and a pilot from LHR to JFK (i.e., WB) could detour southward rather than northward of the jet streak. This routing eventually gives social benefits by producing efficient and safe flights, and also gives reduced impacts on environment, although more impacts from $NO_x$-induced $O_3$ and water vapor in the stratosphere, contrail formations in Ice Super Saturated Regions, and noise near airports should be also considered for climate-optimal and environmentally-sound WORs (e.g., Köhler et at. 2008; Grewe and Stenke 2008; Grewe et al., 2014). WORs and their adverse CAT encounters can be changed by upper-level weather patterns, which can be also applied to future climate scenarios (e.g., Williams and Joshi

13

1    2013). Further studies to look at other types of CAT indicators related to spontaneous

2    imbalance (e.g., Knox et al. 2008), mountain waves (e.g., Kim and Chun 2010; Sharman

3    et al. 2011), and deep convection (e.g., Kim and Chun 2012; Kim et al. 2014; Trier and

4    Sharman 2010) or a combined indicator like Graphical Turbulence Guidance (GTG;

5    Sharman et al. 2006; Kim et al. 2011; Gill 2014) should be priorities for future research.

6    Other types of weather constraints such as deep convection, icing, volcano ash, as well

7    as climate concerns like $NO_2$ and water vapor emissions in stratosphere and contrail

8    formations (e.g., Grewe and Stenke 2008; Grewe et al., 2014), can be also considered in

9    optimizing routes using similar techniques in the future.

10

1    **References**

2    Barnston, A. G., and R. E. Livezey, R. E., 1987: Classification, seasonality and

3        persistence of low-frequency atmospheric circulation patterns. *Mon. Wea. Rev.,* **115**,

4        1083-1126.

5    Bryson, A. E., and Y. C. Ho, Y. C., 1975: *Applied Optimal Control*, Taylor and Fancis,

6        481 pp.

7    Ellrod, G. P., and D. I. Knapp, D. I., 1992: An objective clear-air turbulence forecasting

8        technique: Verification and operational use. *Wea. Forecasting*., **7**, 150–165.

9    Irvine, E. A., B. J. Hoskins, K. P. Shine, R. W. Lunnon, and C. Froemming, 2012:

10       Characterizing North Atlantic weather patterns for climate-optimal aircraft routing.

11       *Meteorological Applications,* **20**, 80-93. DOI: 10.1002/met.1291.

12   Jaeger, E. B., and M. Sprenger, M., 2007: A northern-hemispheric climatology of

13       indices for clear air turbulence in the tropopause region derived from ERA40 re-

14       analysis data. *J. Geophys. Res*., **112**, D20106. doi:10.1029/2006JD008189.

15   Gill, P. G., 2014: Objective verification of World Area Forecast Centre clear air

16       turbulence forecasts, *Meteorological Applications.,* **21**, 3-11. DOI:

17       10.1002/met.1288.

18   Grewe, V. and Stenke, A., 2008: AirClim: an efficient tool for climate evaluation of

19       aircraft technology, *Atmos. Chem. Phys.*, **8**, 4621-4639, doi:10.5194/acp-8-4621-

20       2008.

15

1   Grewe, V., T. Champougny, S. Matthes, C. Frömming, S. Brinkop, O. A. Søvde, E. A.

2       Irvine, L. Halscheidt, 2014: Reduction of the air traffic's contribution to climate

3       change: A REACT4C case study. *Atmospheric Environment*, **94,** 616-625.

4   Karnauskas, K. B., J. P. Donnelly, H. C. Barkley, and J. E. Martin, 2015: Coupling

5       between air travel and climate. *Nature Clim. Change.* doi:10.1038/nclimate2715**.**

6   Kim, J.-H., and H.-Y. Chun, 2010: A numerical study of clear-air turbulence (CAT)

7       encounters over South Korea on 2 April 2007. *J. Appl. Meteor. Climatol*, **49,** 2381-

8       2403.

9   Kim, J.-H., and H.-Y. Chun, H.-Y., 2011: Statistics and possible sources of

10      aviation turbulence over South Korea. *J. Appl. Meteor. Climatol.,* **50**(2),

11      311-324.

12  Kim, J.-H., H.-Y. Chun, R. D. Sharman, T. L. Keller, 2011: Evaluations of Upper-Level

13      Turbulence Diagnostics Performance Using the Graphical Turbulence Guidance

14      (GTG) System and Pilot Reports (PIREPs) over East Asia. *J. Appl. Meteor.*

15      *Climatol.,* **50**, 1936-1951.

16  Kim, J.-H., and Chun, H.-Y., 2012: A Numerical Simulation of Convectively Induced

17      Turbulence above Deep Convection. *J. Appl. Meteor. Climatol.*, **51**, 1180-1200.

18  Kim, J.-H., Chun, H.-Y., Sharman, R. D., and Trier, S. B., 2014: The Role of Vertical

19      Shear on Aviation Turbulence within Cirrus Bands of a Simulated Western Pacific

20      Ocean. *Mon. Wea. Rev.*, **142**, 2794-2813.

21  Kim, J.-H., W. N. Chan, B. Sridhar, and R. D. Sharman, 2015: Combined winds and

22      turbulence prediction system for automated Air-Traffic Management applications. *J.*

23      *Appl. Meteor. Climatol.,* **54**, 766-784.

1 Köhler, M. O., G. Rädel, O. Dessens, K. P. Shine, H. L. Rogers, O. Wild, and J. A.

2 Pyle, 2008: Impact of perturbations to nitrogen oxide emissions from global aviation,

3 *J. Geophys. Res.*, **113**, D11305, doi:10.1029/2007JD009140.

4 Krozel, J., V. Klimenko, and R. D. Sharman, 2011: Analysis of Clear-Air Turbulence

5 Avoidance Maneuvers. *Air Traffic Control Quart.*, **4(2)**, 147-168.

6 Knox, J. A., D. W. McCann, and P. D. Williams, 2008: Application of the Lighthill–

7 Ford theory of spontaneous imbalance to clear-air turbulence forecasting. *J. Atmos.*

8 *Sci.*, **65**, 3292–3304.

9 Lee, D. S., D. W. Fahey, P. M. Forster, P. J. Newton, R. C. N. Wit, L. L. Lim, B. Owen,

10 and R. Sausen, 2009: Aviation and global climate change in the 21st century.

11 *Atmospheric Environment*, **43,** 3520-3537.

12 Lee, D. S., G. Pitari, V. Grewe, K. Gierens, J. E. Penner, A. Petzold, M. J. Prather, U.

13 Schumann, A. Bais, T. Bernsten, D. Iachetti, L. L. Lim, and R. Sausen, 2010:

14 Transport impacts on atmosphere and climate: Aviation. *Atmospheric Environment*,

15 **44,** 4678-4734.

16 Lester, P. F.: Turbulence, 1994: *Turbulence: A new perspective for pilots*. Jeppesen

17 Sanderson, Inc., 212 pp.

18 Ng, H. K., B. Sridhar, and S. Grabbe, 2012: A practical approach for optimizing aircraft

19 trajectories in winds. *31$^{st}$ Digital Avionics Systems Conference, Institute of*

20 *Electrical and Electronics Engineers*, 14 pp. [Available online at http://

21 www.aviationsystemsdivision.arc.nasa.gov/publications/2012/

22 DASC2012_Ng.pdf.].

23 Schumann, U., and K. Graf., 2013: Aviation-induced cirrus and radiation changes at

1  diurnal timescales. *J. Geophys. Res.*, **118(5)**:2404–2421. doi:10.1002/jgrd.50184.

2  Sharman, R. D., C. Tebaldi, G. Wiener, J. Wolff, 2006: An integrated approach to mid-
3  and upper-level turbulence forecasting. *Wea. Forecasting,* **21(3)**, 268-287.

4  Sharman, R. D., Doyle, J. D., Shapiro, M. A., 2011: An Investigation of a Commercial
5  Aircraft Encounter with Severe Clear-Air Turbulence over Western Greenland. *J.*
6  *Appl. Meteor. Climatol.*, **51(1)**, 311-324.

7  Sridhar, B., H. K. Ng, and N. Y. Chen, 2011: Aircraft trajectory optimization and
8  contrails avoidance in the presence of winds. *J. Guidance, Control, Dyn.*, **34**, 1577–
9  1584, doi:10.2514/1.53378.

10  Williams, P. D., 2016: Transatlantic flight times and climate change. *Environmental*
11  *Research Letters*, in press.

12  Williams, P. D., and M. M. Joshi, 2013: Intensification of winter transatlantic aviation
13  turbulence in response to climate change. *Nature Climate Change,* **3**(7) 644–648.
14  doi:10.1038/nclimate1866.

15  Wolff, J. K., and R. D. Sharman, 2008: Climatology of upper-level turbulence
16  over the Contiguous United States. *J. Appl. Meteor. Climatol.,* **47**, 2198-2214.

1 **Table Captions**

2    **Table 1.** Median values of Turbulence Index 1 (TI1; $s^{-2}$) and probability for

3 Moderate-Or-Greater (MOG)-level turbulence along the Eastbound (EB) and

4 Westbound (WB) Wind-Optimal Routes during +North Atlantic Oscillation (+NAO)

5 phase in December 2004 – February 2005 (DJF04-05) and (–NAO) phase in December

6 2009 – February 2010 (DJF09-10).

7

8

1 **Figure Captions**

2 **Figure 1.** Schematic of an aircraft flying horizontally on an Earth surface with a true

3 airspeed ($V_t$) and heading angle ($\alpha$) during a certain period of time ($\Delta t$). Here, $\lambda$ and $\phi$

4 are longitudinal and latitudinal directions, respectively.

5 **Figure 2.** (Upper) (a) Eastbound Wind-Optimal Route (WOR; bold blue) and (b)

6 Westbound WOR (bold red) between JFK and LHR with candidate trajectories (gray

7 lines) from different initial heading angles ranging Great-Circle heading angle ($\alpha_{GC}$)

8 − 45° to $\alpha_{GC}$ + 45° with 2.5° bins and horizontal winds vectors at 00 (left) and 12

9 (right) UTC 3 January 2005 at 250 hPa (about z = 11 km or 34 000 ft). (Lower)

10 Corresponding minimum distance (km) between the trajectories and destination

11 airport for (c) Eastbound and (d) Westbound. Reference wind vectors on bottom

12 right in upper panel are 50 m s$^{-1}$. The optimal flight routes for eastbound and

13 westbound having the minimum time and distance are depicted as blue (Eastbound)

14 and red (Westbound) lines in left and right plots. In all plots, the black line is the

15 great circle route between JFK and LHR.

16 **Figure 3.** (Upper) Averaged horizontal wind speed (shadings from 10 to 50 m s$^{-1}$ with

17 10 m s$^{-1}$ interval) and variations of the WORs at 250 hPa between JFK and LHR for

18 (Middle) Eastbound (blue-dotted lines) and (Lower) Westbound (red-dotted lines)

19 during (a, c, e) December 2004 – February 2005 and (b, d, f) December 2009 –

20 February 2010. Great Circle between JFK and LHR is depicted as a reference (black

21 line) in all plots.

22 **Figure 4.** Bar charts of the mean, mean ± 2 stds, and minimum and maximum values of

23 the travel times along the Eastbound (WOREB) and Westbound (WORWB) Wind-

24 Optimal Routes between JFK and LHR shown in Fig. 3 during the (two leftmost)

1  +North Atlantic Oscillation (+NAO) phase in December 2004 – February 2005

2  (DJF04-05) and (two rightmost) –NAO phase in December 2009 – February 2010

3  (DJF09-10).

4  **Figure 5.** Shadings of averaged Turbulence index 1 (TI1; $s^{-2}$) for (a) +North Atlantic

5  Oscillation (+NAO) phase in December 2004 – February 2005 (DJF04-05) and (b) –

6  NAO phase in December 2009 – February 2010 (DJF09-10), and (c) their difference.

7  (d) Eastbound (blue) and Westbound (red) Wind-Optimal Routes with TI1 (shading)

8  and horizontal wind vectors at 250 hPa level between JFK and LHR on 3 January

9  2005. It is noted that the shading levels for the TI1 in upper and lower panels are

10  different.

11  **Figure 6.** Probability Density Function (PDF) for Turbulence index 1 (TI1; $s^{-2}$) along the

12  Eastbound (blue bars) and Westbound (red bars) Wind-Optimal Routes (WORs) during

13  +North Atlantic Oscillation (+NAO) phase in December 2004 – February 2005 (DJF04-05).

14  Overlaps of the PDFs between Eastbound and Westbound WORs are in orange-color bars.

15

16

17

18

19

20

21

22

1  **Table 1.** Median values of Turbulence Index 1 (TI1; s$^{-2}$) and probability for Moderate-

2  Or-Greater (MOG)-level turbulence along the Eastbound (EB) and Westbound (WB)

3  Wind-Optimal Routes during +North Atlantic Oscillation (+NAO) phase in December

4  2004 – February 2005 (DJF04-05) and (–NAO) phase in December 2009 – February

5  2010 (DJF09-10).

6

|  | DJF 04-05 (+NAO) | | DJF 09-10 (-NAO) | |
|---|---|---|---|---|
|  | Median (s$^{-2}$) | MOG (%) | Median (s$^{-2}$) | MOG (%) |
| East Bound (EB) | $2.34 \times 10^{-8}$ | 1.02 | $2.59 \times 10^{-8}$ | 1.31 |
| West Bound (WB) | $2.15 \times 10^{-8}$ | 0.92 | $2.29 \times 10^{-8}$ | 0.81 |

7

8

9

1
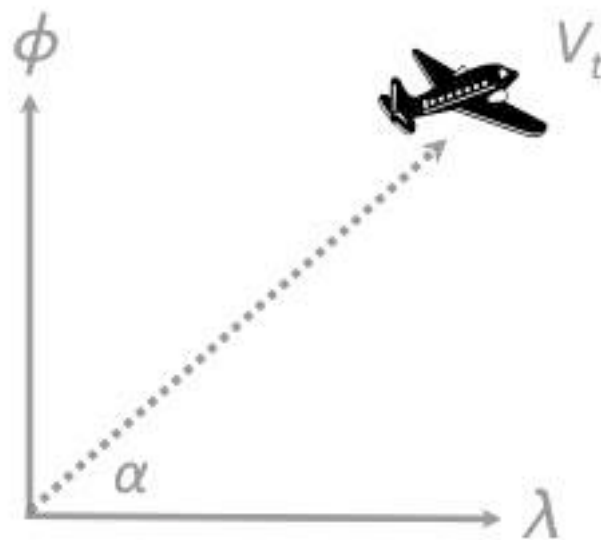
1
2
3   **Figure 1.** Schematic of an aircraft flying horizontally on an Earth surface with a true airspeed
4   ($V_t$) and heading angle ($\alpha$) during a certain period of time ($\Delta t$). Here, $\lambda$ and $\phi$ are
5   longitudinal and latitudinal directions, respectively.
6

1
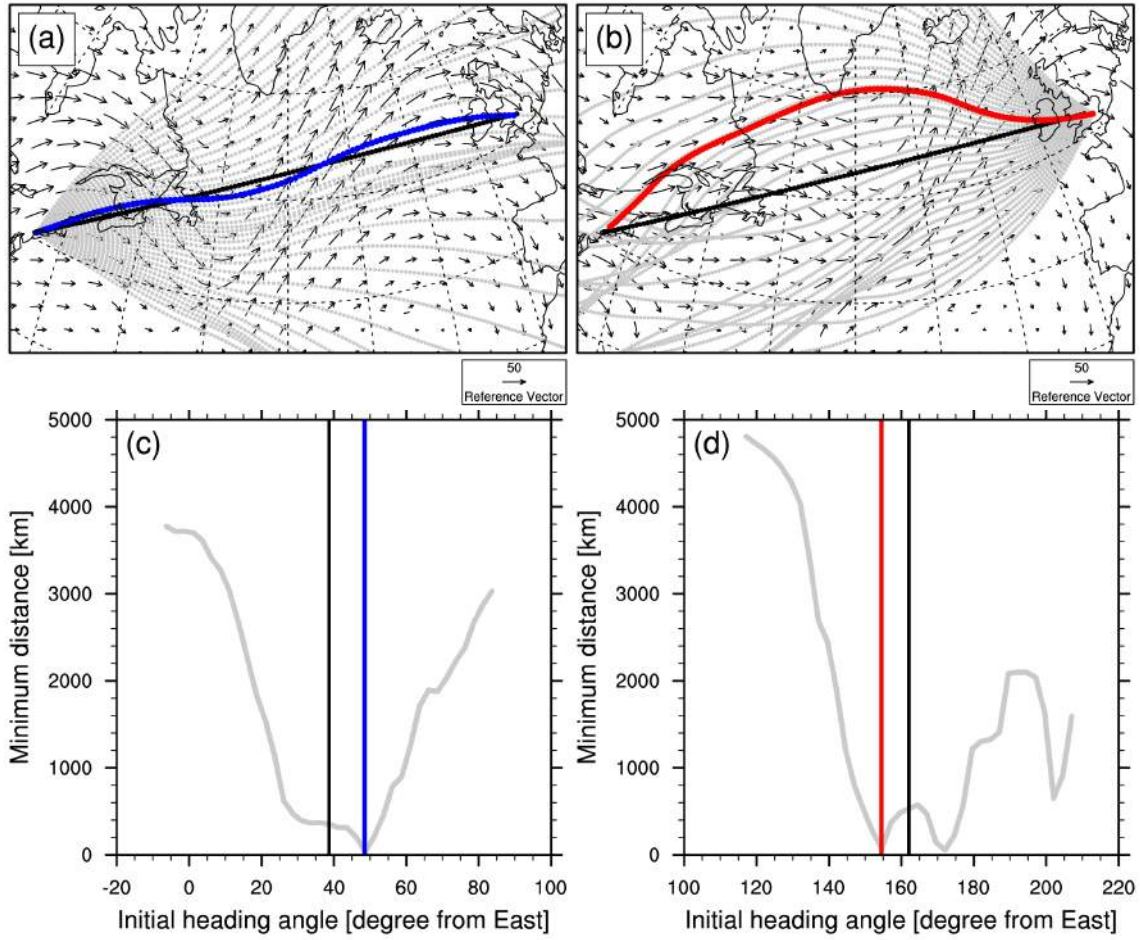
**Figure 2.** (Upper) (a) Eastbound Wind-Optimal Route (WOR; bold blue) and (b) Westbound
WOR (bold red) between JFK and LHR with candidate trajectories (gray lines) from
different initial heading angles ranging Great-Circle heading angle ($\alpha_{GC}$) − 45° to $\alpha_{GC}$ + 45°
with 2.5° bins and horizontal winds vectors at 00 (left) and 12 (right) UTC 3 January 2005
at 250 hPa (about z = 11 km or 34 000 ft). (Lower) Corresponding minimum distance (km)
between the trajectories and destination airport for (c) Eastbound and (d) Westbound.
Reference wind vectors on bottom right in upper panel are 50 m s$^{-1}$. The optimal flight
routes for eastbound and westbound having the minimum time and distance are depicted as
blue (Eastbound) and red (Westbound) lines in left and right plots. In all plots, the black
line is the great circle route between JFK and LHR..
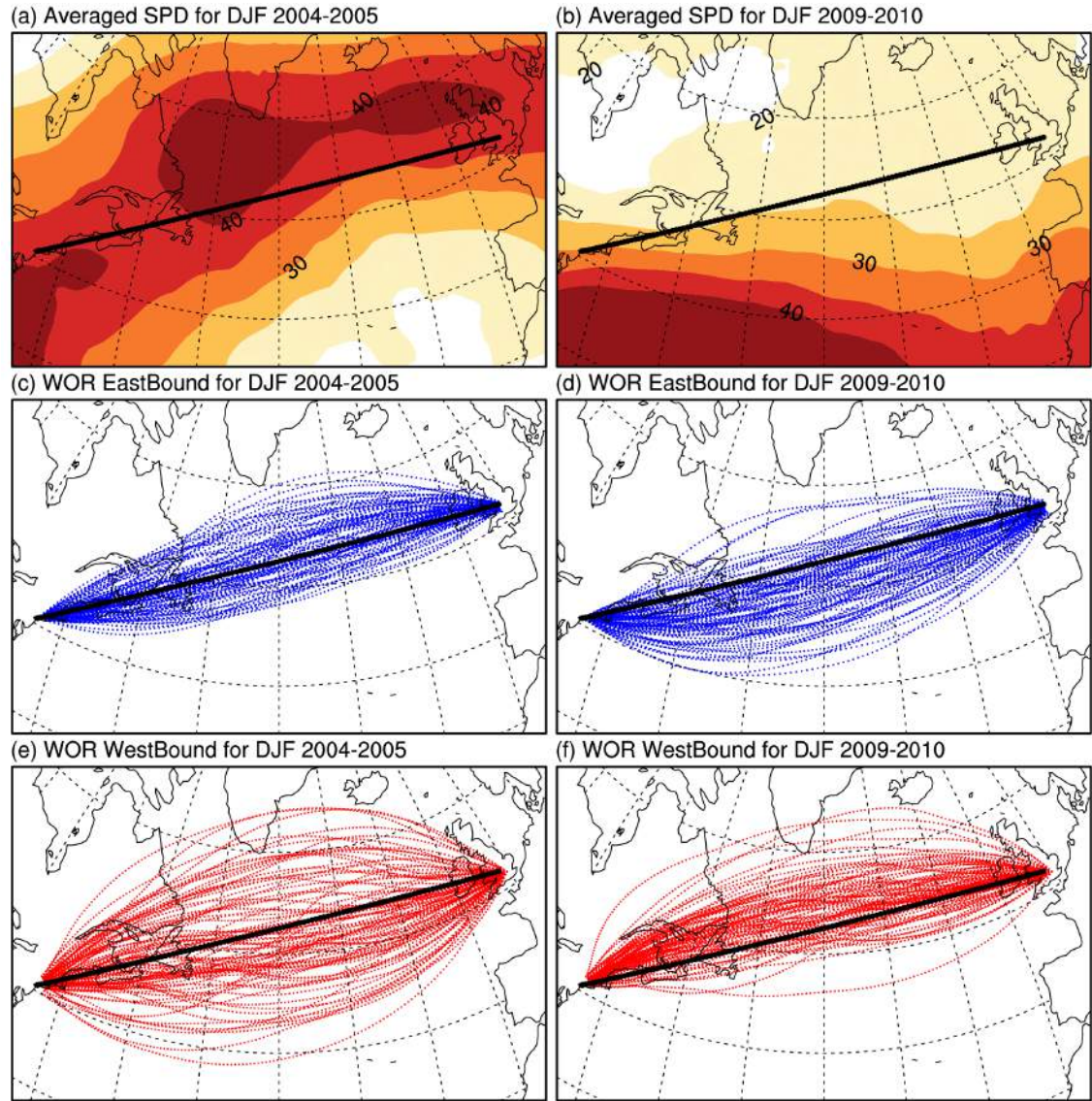
**Figure 3.** (Upper) Averaged horizontal wind speed (shadings from 10 to 50 m s$^{-1}$ with 10 m s$^{-1}$ interval) and variations of the WORs at 250 hPa between JFK and LHR for (Middle) Eastbound (blue-dotted lines) and (Lower) Westbound (red-dotted lines) during (a, c, e) December 2004 – February 2005 and (b, d, f) December 2009 – February 2010. Great Circle between JFK and LHR is depicted as a reference (black line) in all plots.
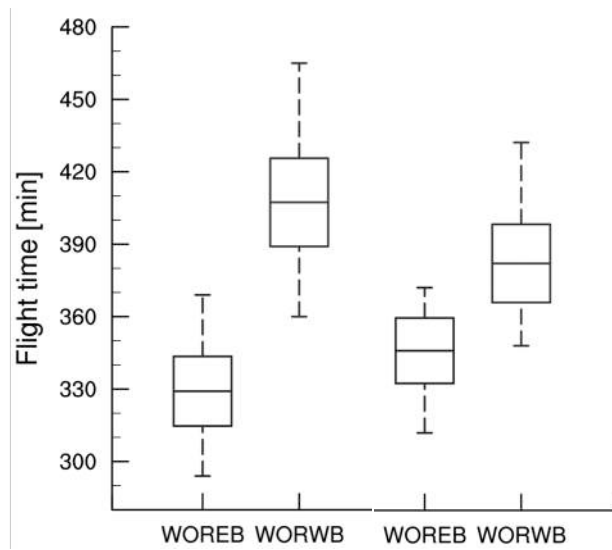
**Figure 4.** Bar charts of the mean, mean ± 2 stds, and minimum and maximum values of the travel times along the Eastbound (WOREB) and Westbound (WORWB) Wind-Optimal Routes between JFK and LHR shown in Fig. 3 during the (two leftmost) +North Atlantic Oscillation (+NAO) phase in December 2004 – February 2005 (DJF04-05) and (two rightmost) –NAO phase in December 2009 – February 2010 (DJF09-10).
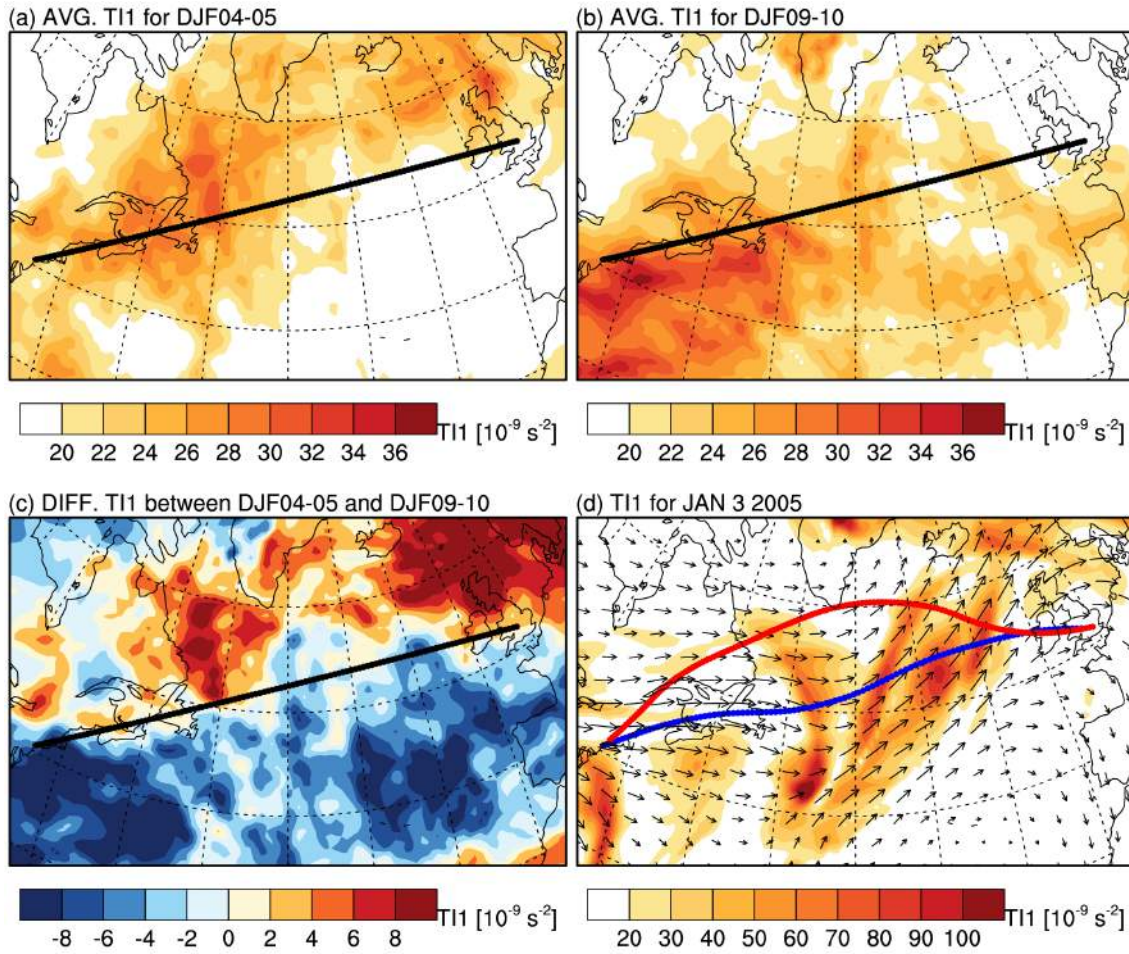
**Figure 5.** Shadings of averaged Turbulence index 1 (TI1; s$^{-2}$) for (a) +North Atlantic Oscillation (+NAO) phase in December 2004 – February 2005 (DJF04-05) and (b) –NAO phase in December 2009 – February 2010 (DJF09-10), and (c) their difference. (d) Eastbound (blue) and Westbound (red) Wind-Optimal Routes with TI1 (shading) and horizontal wind vectors at 250 hPa level between JFK and LHR on 3 January 2005. It is noted that the shading levels for the TI1 in upper and lower panels are different.
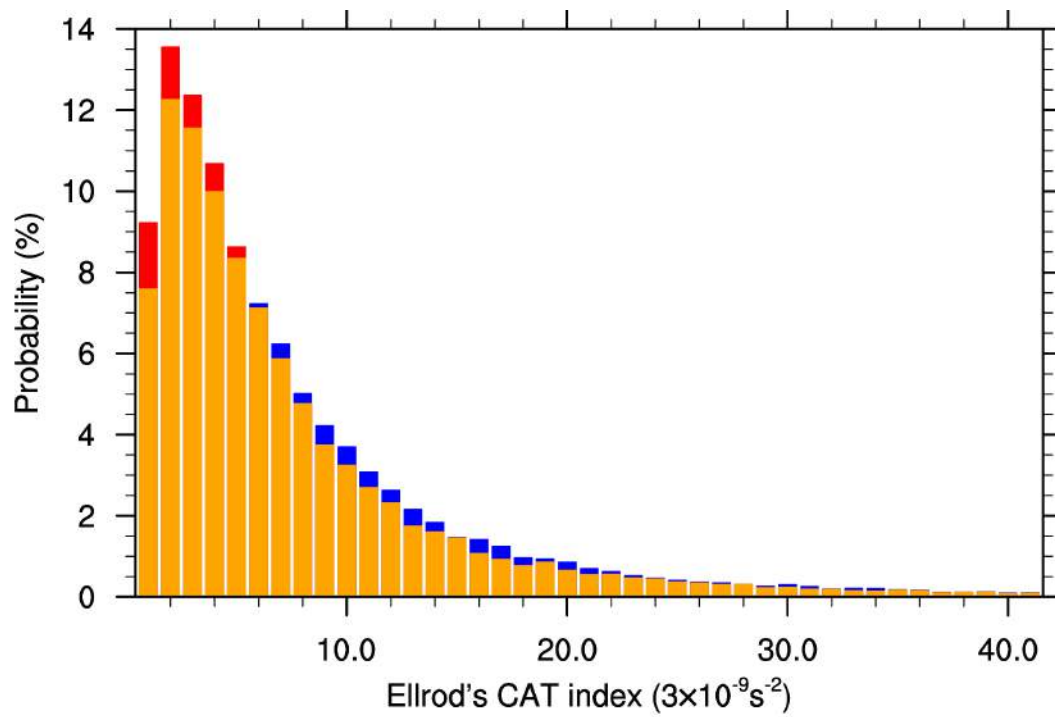
1
2
3  **Figure 6.** Probability Density Function (PDF) for Turbulence index 1 (TI1; s$^{-2}$) along the
4  Eastbound (blue bars) and Westbound (red bars) Wind-Optimal Routes (WORs) during +North
5  Atlantic Oscillation (+NAO) phase in December 2004 – February 2005 (DJF04-05). Overlaps of
6  the PDFs between Eastbound and Westbound WORs are in orange-color bars.
7

8